

The Nature of Nearby Counterparts to Intermediate Redshift Luminous Compact Blue Galaxies

I. Optical/H I Properties and Dynamical Masses

C. A. Garland¹

Institute for Astronomy, University of Hawai‘i, 2680 Woodlawn Drive, Honolulu, HI 96822

cagarland@alum.colby.edu

D. J. Pisano²

CSIRO Australia Telescope National Facility, P.O. Box 76, Epping, NSW 1710, Australia

DJ.Pisano@csiro.au

J. P. Williams

Institute for Astronomy, University of Hawai‘i, 2680 Woodlawn Drive, Honolulu, HI 96822

jpw@ifa.hawaii.edu

R. Guzmán

*Department of Astronomy, University of Florida, 211 Bryant Space Science Center,
P.O. Box 112055, Gainesville, FL 32611-2055*

guzman@astro.ufl.edu

and

F. J. Castander

*Institut d'Estudis Espacials De Catalunya/CSIC, Gran Capità 2-4, E-08034 Barcelona,
Spain*

fjc@ieec.fcr.es

ABSTRACT

¹Present address: Natural Sciences Department, Castleton State College, Castleton, VT 05735

²Bolton Fellow & NSF MPS Distinguished International Postdoctoral Research Fellow

We present single-dish H I spectra obtained with the Green Bank Telescope, along with optical photometric properties from the Sloan Digital Sky Survey, of 20 nearby ($D \lesssim 70$ Mpc) Luminous Compact Blue Galaxies (LCBGs). These $\sim L^*$, blue, high surface brightness, starbursting galaxies were selected with the same criteria used to define LCBGs at higher redshifts. We find these galaxies are gas-rich, with M_{HI} ranging from 5×10^8 to $8 \times 10^9 M_\odot$, and $M_{HI} L_B^{-1}$ ranging from 0.2 to $2 M_\odot L_\odot^{-1}$, consistent with a variety of morphological types of galaxies. We find the dynamical masses (measured within R_{25}) span a wide range, from 3×10^9 to $1 \times 10^{11} M_\odot$. However, at least half have dynamical mass-to-light ratios smaller than nearby galaxies of all Hubble types, as found for LCBGs at intermediate redshifts. By comparing line widths and effective radii with local galaxy populations, we find that LCBGs are consistent with the dynamical mass properties of Magellanic (low luminosity) spirals, and the more massive irregulars and dwarf ellipticals, such as NGC 205.

Subject headings: galaxies: evolution — galaxies: fundamental parameters — galaxies: ISM — galaxies: kinematics and dynamics — galaxies: starburst

1. Introduction

1.1. Luminous, compact, star forming galaxies in the distant Universe

The Hubble Space Telescope and advances in ground based observing have greatly increased our knowledge of the galaxy population in the distant Universe. However, the nature of these galaxies and their evolutionary connections to local galaxies remain poorly understood. Luminous, compact, star forming galaxies appear to represent a prominent phase in the early history of galaxy formation (Jangren et al. 2004). In particular:

- The number density of luminous, compact star forming galaxies rises significantly out to $z \sim 1$ (Koo et al. 1994; Guzmán et al. 1997; Phillips et al. 1997; Lilly et al. 1998; Mallén-Ornelas et al. 1999).
- The Lyman Break galaxies at $z > 2$ seen in the Hubble Deep Field are characterized by very compact cores and a high surface brightness (Giavalisco, Steidel & Macchetto 1996; Lowenthal et al. 1997; Weedman et al. 1998).
- Sub-millimeter imaging has revealed distant galaxies ($z \sim 2-4$), half of them compact objects, which may be responsible for as much as half of the total star formation rate in the early Universe (Smail et al. 1998).

However, little is definitively known of their physical properties, or how they are related to subsets of the local galaxy population.

A classification for known examples of intermediate redshift ($0.4 \lesssim z \lesssim 0.7$) luminous, blue, compact galaxies, such as Blue Nucleated Galaxies, Compact Narrow Emission Line Galaxies, and Small Blue Galaxies, has been developed by Jangren et al. (2004) in order to be able to choose samples over a wide redshift range. They have found that the bulk of these galaxies, collectively termed Luminous Compact Blue Galaxies (LCBGs), can be distinguished quantitatively from local normal galaxies by their blue color, small size, high luminosity, and high surface brightness. (See §2.1 for more detail.)

From studies at intermediate redshifts, it has been found that LCBGs are a heterogeneous class of vigorously starbursting, high metallicity galaxies with an underlying older stellar population (Guzmán et al. 1996, 1998). While common at intermediate redshifts, they are rare locally (Mallén-Ornelas et al. 1999) and little is known about the class as a whole, nor their evolutionary connections to other galaxies. LCBGs undergo dramatic evolution: At $z \sim 1$, they are numerous and have a total star formation rate density equal to that of grand-design spirals at that time. However, by $z \sim 0$, the number density and star formation rate density of LCBGs has decreased by at least a factor of ten (Marzke et al. 1994; Guzmán et al. 1997). Since the LCBG population is morphologically and spectroscopically diverse, these galaxies are unlikely to evolve into one homogeneous galaxy class. Koo et al. (1994) and Guzmán et al. (1996) suggest that a subset of LCBGs at intermediate redshifts may be the progenitors of local low-mass dwarf elliptical galaxies such as NGC 205. Alternatively, Phillips et al. (1997) and Hammer et al. (2001) suggest that others may be disk galaxies in the process of building a bulge to become local L* spiral galaxies.

Clearly, to determine the most likely evolutionary scenarios for intermediate redshift LCBGs, it is necessary to know their masses and the timescale of their starburst activity. Are they comparable to today’s massive or low-mass galaxies? Are they small starbursting galaxies which will soon exhaust their gas and eventually fade? Or are they larger galaxies with only moderate amounts of star formation? Only kinematic line widths that truly reflect the masses of these galaxies, as well as measures of their gas content and star formation rates, can answer these questions. Using ionized gas emission line widths, Koo et al. (1994), Guzmán et al. (1996), and Phillips et al. (1997), have found that LCBGs have mass-to-light ratios approximately ten times smaller than typical local L* galaxies. However, since ionized gas emission lines may originate primarily from the central regions of galaxies, their line widths may underestimate the gravitational potential (Barton & van Zee 2001). H I emission lines provide a better estimate of the total galaxy mass as they measure the gravitational potential out to larger galactic radii. Observations of both H I and CO (the best tracer

of cold H_2), combined with star formation rates, are necessary to estimate the starburst timescales.

1.2. A local sample of LCBGs

With current radio instrumentation, H I and CO can only easily be measured in very nearby LCBGs, at distances $\lesssim 150$ Mpc for H I, and $\lesssim 70$ Mpc for CO. Therefore, to understand the nature and evolutionary possibilities of higher redshift LCBGs, we have undertaken a survey in H I 21 cm emission and multiple rotational transitions of CO of a sample of 20 local LCBGs, drawn from the Sloan Digital Sky Survey (York et al. 2000). This work, Paper I, reports the optical photometric properties of our sample and the results of the H I 21 cm portion of the survey, including dynamical masses and comparisons with local galaxy types. Paper II (Garland et al. 2004) will report the results of a survey of the molecular gas conditions. Knowledge of the dynamical masses, combined with gas masses and star formation rates, constrains the evolutionary possibilities of these galaxies.

Nearby blue compact galaxies (BCGs) have been studied extensively at radio and optical wavelengths since Zwicky (1964) originated the term “compact galaxy” and Sargent (1970) distinguished between “red” and “blue” compact galaxies. The term BCG typically refers to galaxies with a compact nature, a high mean surface brightness, and emission lines superposed on a blue continuum. However, many different selection criteria have been used, leading to various definitions of BCGs and samples with a range of properties. For example, the term “dwarf” has been used to mean BCGs fainter than -17 (e.g. Thuan & Martin 1981; Kong & Cheng 2002) or -18 blue magnitudes (e.g. Taylor et al. 1994), or an optical diameter less than 10 kpc (Campos-Aguilar et al. 1993). The term “blue” has been used to mean blue on the Palomar Sky Survey Plate (e.g. Gordon & Gottesman 1981), or to have emission lines superposed on a blue background (e.g. Thuan & Martin 1981). The term “compact” has been used to mean smaller than 1 kpc in optical diameter (e.g. Thuan & Martin 1981), or qualitatively compact (e.g. Doublier et al. 1997). Some, for example Thuan & Martin (1981), began using the term Blue Compact Dwarf to refer to the common low luminosity, low metallicity BCGs. As high luminosity ($\sim L^*$), nearby BCGs are rare, many began to use the term Blue Compact Dwarf for all nearby BCGs, regardless of luminosity.

There are only a few of the rare local LCBGs (by the Jangren et al. (2004) definition) in previous BCG surveys. Note that Bergvall & Östlin (2002) have recently been studying local luminous BCGs. However, their selection criteria are not as stringent as that of Jangren et al. (2004), and they have been focusing on very low metallicity (less than 15% solar) galaxies. Intermediate redshift LCBGs with rest-frame properties matching the class definition of

Jangren et al. (2004) have metallicities at least 40% solar (Guzmán et al. 1996). Four of our local LCBGs have metallicities available in the literature, which range from 40 – 70 % solar (Hunter & Gallagher 1986; Calzetti 1997). By using the selection criteria of Jangren et al. (2004), we ensure that our study is of those local LCBGs defined to be analogs to the widely studied higher redshift LCBGs.

The observations, including sample selection and data reduction, are described in §2. The optical photometric properties, H I 21 cm spectra, measurements, and derived properties are presented in §3, and analyzed in §4. We compare the derived physical properties to local normal galaxies and higher redshift LCBGs in §5, and conclude in §6. We assume $H_0 = 70 \text{ km s}^{-1} \text{ Mpc}^{-1}$ throughout. When we compare our results to those of other authors, we scale their results to this value.

2. The Observations

2.1. Sample Selection

2.1.1. Selection Criteria

When Jangren et al. (2004) compared intermediate redshift LCBGs with local normal galaxies, they found that LCBGs can be isolated quantitatively on the basis of color, surface brightness, image concentration, and asymmetry. Color and surface brightness were found to give the best leverage for separating LCBGs from normal galaxies. Specifically, LCBGs can be defined by a region limited to $B-V < 0.6$, and a B-band surface brightness within the half-light radius, SBe, brighter than $21 \text{ B-mag arc sec}^{-2}$. This simple definition differs only slightly from the formal definition in Jangren et al. (2004) which uses a color-dependent SBe. Jangren et al. (2004) also applied a luminosity cut-off of 25% L^* ($M_B < -18.5$), to distinguish LCBGs from blue compact galaxies. LCBGs are not so extreme that they are completely separated from the continuum of normal galaxies. The sharp borders used to classify them are artificial, but serve the purpose of defining similar objects over a range of redshifts. LCBGs at intermediate redshifts ($z \sim 0.6$) can be studied in deep spectroscopic surveys ($I \sim 24$), while the brightest LCBGs at high redshifts ($z \sim 3$) require very deep spectroscopic surveys ($I \sim 26$). Therefore, LCBGs selected in this manner are observable over a wide range of redshifts.

Using these color, surface brightness, and luminosity criteria, we selected our sample of local LCBGs from the Sloan Digital Sky Survey (SDSS). Begun in 2000, this survey will ultimately image one quarter of the sky using a large format CCD camera on a 2.5 m telescope

at Apache Point Observatory in New Mexico. Images are taken in five broad bands (u, g, r, i, z) which range from 3540 Å (u) to 9130 Å (z). The survey has a limiting magnitude of 22.2 in g (4770 Å) and r (6230 Å), our two bands of interest. After searching through approximately one million galaxies (\sim 1500 degree² on the sky), we identified only 16 nearby ($D \lesssim 70$ Mpc) LCBGs. This distance cut-off was chosen to ensure our galaxies could be detected quickly in both H I and CO. We added four Markarian galaxies from the literature which fulfilled our selection criteria and were not yet surveyed by SDSS, for a total of 20 local LCBGs. The color and surface brightness characteristics of our local sample, as well as higher redshift ($0.4 \lesssim z \lesssim 1$) samples of LCBGs, are compared to other nearby galaxies in Figure 1. We note that while our sample is not complete, it is representative of local LCBGs (see Castander et al. 2004).

2.1.2. Galaxy Properties

As at higher redshifts (Phillips et al. 1997), our local LCBG sample is a morphologically heterogeneous mixture of galaxies, including Sb to Sc spirals, S0 galaxies, polar ring galaxies, peculiar galaxies, and H II liners and starbursts, as classified by HyperLeda¹ and the NASA/IPAC Extragalactic Database² (NED). Approximately one quarter of these galaxies are not classified in either database. Roughly one third are members of multiple, sometimes interacting or merging, systems. SDSS and Digitized Sky Survey images of our sample of 20 galaxies are shown in Figures 2 and 3. The properties of our sample of local LCBGs are described below, and listed in Table 1.

Source. Full SDSS galaxy designation of the form SDSS JHHMMSS.ss+DDMMSS.s, in the J2000 system. In the remainder of the paper, individual galaxies are referred to by an abbreviated SDSS name of the form SDSSJHHMM+DDMM. The four non-SDSS galaxies are referred to by their Markarian (Mrk) names.

Alternate Name. Mrk and/or NGC designation, if any.

D_{OPT} . Hubble distance, in Mpc, calculated from the optical redshift (from SDSS, except for the non-SDSS galaxies for which we use NED redshifts.)

M_B . Absolute blue magnitude calculated from the apparent blue magnitude, m_B , using

¹<http://www-obs.univ-lyon1.fr/hypercat/>

²<http://nedwww.ipac.caltech.edu/>

D_{OPT} . For the SDSS galaxies, $m_B = g + 0.30(g-r) + 0.18^3$. The r and g magnitudes were calculated from the SDSS “petrosian” and “model” magnitudes: $r = r(\text{petro})$ and $g = r(\text{petro}) - [r(\text{model}) - g(\text{model})]$ (Stoughton 2002). The SDSS Galactic reddening corrections were applied, but no K corrections were applied as our galaxies are nearby, and many are of unknown spectral type. The K correction is at most 0.015 magnitudes in r and 0.038 magnitudes in g (Poggianti 1997). No correction was applied for extinction due to inclination, also because of the uncertainty in spectral types. For the non-SDSS galaxies, the “total apparent blue magnitudes” were used from HyperLeda, and corrected for Galactic reddening using extinction values from NED.

$B-V$. The color transformation is $B-V = 0.900(g-r) + 0.145^5$, where the magnitudes were calculated as above, for the SDSS galaxies. The “total $B-V$ colors” from HyperLeda were used for the non-SDSS galaxies. They were corrected for reddening using extinction values from NED.

SBe. Average surface brightness in the B band within the half light or effective radius in B-mag arc sec $^{-2}$. For the SDSS galaxies, $SBe(B) = m_B + 2.5 \log [2\pi r_e^2(B)]$, where $r_e(B)$, the effective or half-light radius in the B band, was calculated from the “petrosian” effective radii in the g and r bands [$r_e(B) = 1.30 r_e(g) - 0.300 r_e(r)$]⁵. We corrected SBe for cosmological dimming by subtracting $7.5 \log(1+z)$, where the redshift, z , was calculated using the H I velocity (§3.1). For the non-SDSS galaxies, we used SBe from HyperLeda (termed the “mean effective surface brightness”), and then corrected it for cosmological dimming in the same way.

NED Type. Morphological type as given by NED, which does not use a homogeneous system.

HyperLeda Type. Morphological type as given by HyperLeda, which uses the de Vaucouleurs et al. (1991) system.

Other Sources in Beam? Indicates whether or not each galaxy has other sources at similar velocities within the 9'.2 beam of the Green Bank Telescope (used for the H I observations), as given by NED.

³The relationships for m_B , $B-V$, and $r_e(B)$ are based on synthetic spectra which fit the observed spectral energy distribution of LCBGs.

2.1.3. Comparison of SDSS and HyperLeda properties

We compared HyperLeda and SDSS magnitudes for our SDSS selected galaxies to ensure that there are no systematic offsets between the two. Fourteen galaxies had magnitudes measured in both systems. The median difference between SDSS and HyperLeda magnitudes (as calculated in §2.1.2) is 0.1 magnitudes. Since the standard deviation of these differences is ± 0.8 magnitudes, we estimate the uncertainty in the median magnitude difference to be 0.2 magnitudes. Therefore, there is no significant difference between the HyperLeda and SDSS magnitudes. Unfortunately, while fourteen galaxies have magnitudes measured in both systems, only two SDSS selected galaxies have B–V and SBe entries in HyperLeda; for these two galaxies there are no significant differences between the HyperLeda and SDSS values.

2.2. Observations

H I 21 cm observations of 19 of the 20 nearby LCBGs in our sample were made with the 100 meter Green Bank Telescope (GBT) at the National Radio Astronomy Observatory⁴ in Green Bank, West Virginia between 2002 November 30 and December 6. The H I spectrum of SDSSJ0934+0014 was acquired by Fisher (2003) during GBT commissioning on 2001 November 29. The main beam half power width is 9'.2 at 21 cm (Lockman 1998). Both linear and circular polarizations were observed using the L-band receiver (1.15 – 1.73 GHz). Position-switching was used with an offset of $-18'$ in Right Ascension. The spectral processor was used with a bandwidth of 20 MHz (~ 4000 km s $^{-1}$) for most galaxies, although a few were observed with a bandwidth of 5 MHz (~ 1000 km s $^{-1}$). The sample time was 60 s, with each galaxy observed for between 6 and 30 minutes, for a peak signal-to-noise of at least five. The only exceptions were SDSSJ0218–0757 and SDSSJ0222–0830, marginal detections, which were observed for 52 minutes each.

2.3. Reduction

The initial data calibration and reduction was performed using the AIPS++ single dish analysis environment “dish.” The position-switched data were calibrated in the standard way taking the difference of the on and off scans divided by the off scans. The dish package automatically calibrates the data into temperature units using tabulated values for the po-

⁴The National Radio Astronomy Observatory is a facility of the National Science Foundation operated under cooperative agreement by Associated Universities, Inc.

sition of the telescope. The individual scans were then combined and a first order baseline was fit to the line-free regions and removed. Our wide bandwidths ensured a sufficient line-free region. The individual polarizations were then combined, except when one polarization was significantly noisier than the other, or was affected by radio interference. Finally, each spectrum was smoothed to $\sim 12 \text{ km s}^{-1}$ channels using boxcar smoothing.

The rest of the reduction and analysis was done using our own procedures written in Interactive Data Language (IDL). To convert our data from temperature to flux density units, we observed the radio galaxy 3C295. It makes an ideal calibration source as it has not varied by more than $\sim 1\%$ since 1976 for $2.8 \text{ cm} \leq \lambda \leq 21 \text{ cm}$ (Ott et al. 1994). Comparing our observations of 3C295 with those of Ott et al. (1994), we found the gain of the GBT to be 1.9 K Jy^{-1} and applied this calibration to our data. Finally, obvious noise spikes were clipped out of the data. Data of SDSSJ0934+0014, the galaxy observed during telescope commissioning, were reduced and calibrated by Fisher (2003). The spectrum was then smoothed to $\sim 12 \text{ km s}^{-1}$ channels.

The central 800 km s^{-1} of the final H I 21 cm spectra of the 20 local LCBGs are shown in Figure 4. Each galaxy’s velocity calculated from optical redshifts is indicated with a triangle. Dashed lines indicate the 20% crossings used to measure the line widths (§3.1).

3. Results

All 20 galaxies were detected in the 21 cm line of H I, although two, SDSSJ0218–0757 and SDSSJ0222–0830, were only detected at the 3 and 4σ (respectively) level. H I measurements and derived optical and H I quantities are listed in Tables 2, 3 and 4 and described in the following sections. Since the GBT beam is $9'.2$ at 21 cm, the emission from the target galaxies and any other galaxies within the beam and at similar velocities are blended into one spectrum. (See Table 1 for those galaxies with other sources at similar velocities within the GBT beam.)

We find fairly broad H I profiles ($126 \text{ km s}^{-1} < W_{20} < 362 \text{ km s}^{-1}$) and a variety of profile shapes, including double-horned, flat-topped and Gaussian. Over a third of our profiles appear asymmetric and only half of these are from galaxies known to have other sources within the GBT beam. These asymmetries may indicate asymmetries in the gas density distribution and/or disk kinematics, or unidentified galaxies within the beam (Richter & Sancisi 1994).

3.1. Dynamical Masses

Estimates of the dynamical masses of our local sample of LCBGs constrain their evolutionary possibilities. We estimate the dynamical mass, M_{DYN} , within a radius, R , as

$$M_{DYN} (< R) = c_2 \frac{V_{ROT}^2 R}{G} . \quad (1)$$

The constant c_2 is a geometry-dependent factor which depends on the galactic light profile. For example, the King models of Bender, Burstein & Faber (1992) give $0.9 \lesssim c_2 \lesssim 1.5$, depending on the ratio of tidal to core radius. As we do not have information on the light profiles of our galaxy sample, we simply choose $c_2 = 1$.

The line width at 20%, corrected for the effects of inclination, W_{20}^i , is used as a measure of twice the maximum rotational velocity, V_{ROT} (e.g. Tully & Fouqué 1985). W_{20} was measured at the points equal to 20% of the peak flux. The first crossing at 20% on each side of the emission line was used, once the spectrum became distinguishable from the noise. These crossings are indicated by dashed lines in Figure 4. We find W_{20} ranging from $126 - 362 \text{ km s}^{-1}$. When Phillips et al. (1997) studied LCBGs at intermediate redshifts, they found a similar range of line widths, using optical emission lines. The recessional velocities in the barycentric system, V_{BARY} , were calculated as the midpoint between the 20% crossings. The uncertainties listed in Table 2 for W_{20} , V_{BARY} , and the galaxy distance (D) are from uncertainties in measuring the exact W_{20} crossings.

Two galaxies have multiple crossings at the 20% flux level, once the spectrum is distinguishable from the noise. One of these, SDSSJ0834+0139, has a wing on the H I spectrum which extends over 200 km s^{-1} . Neither SDSSJ0834+0139 nor its nearby companion have optical velocities coincident with the peak of the H I spectrum; instead, both have velocities in the wing of the spectrum (see Figure 4). For this reason, we used W_{20} measured from the last crossing, which is at the edge of the wing. The other galaxy with multiple crossings at 20% is SDSSJ0904+5136, which has a low level extension to one side of the spectrum. We used the first crossing at 20%. The uncertainties in these two W_{20} measurements are reflected in the large errors associated with W_{20} and derived quantities. We have initiated an observing program at the Very Large Array (VLA) to map these local LCBGs in H I to disentangle target galaxy emission from any other galaxies in the field, improving the mass estimates.

To correct the line width for the effects of inclination (i), we divided W_{20} by $\sin(i)$, to give W_{20}^i . Each SDSS galaxy's inclination was approximated from the SDSS data by:

$$i = \arccos \frac{\text{minor axis}}{\text{major axis}} . \quad (2)$$

The SDSS isophotal major and minor axes in the g-band (4770 Å) were used, except for SDSSJ0943–0215 where no g band data were available. In that case, r-band (6230 Å) data were used. The SDSS isophotal axes are derived from the ellipticity of the 25 magnitude arc sec^{−2} isophote in each band. Inclinations derived from SDSS isophotal axes in r, i (7630 Å), and z (9130 Å) bands agree with inclinations derived from g-band data to within 8°. The inclinations from HyperLeda were used for the Markarian galaxies. Thirteen of our SDSS galaxies also have inclinations available in HyperLeda, which are calculated from the apparent flattening and morphological type of the galaxies. We estimate the dispersion of the differences between SDSS and HyperLeda inclinations is 12°.

A further correction can be made to W_{20}^i to account for random motions, giving W_R^i . As outlined in Tully & Fouqué (1985),

$$W_R^2 = W_{20}^2 + W_t^2 - 2W_{20}W_t[1 - \exp{-(W_{20}/W_c)^2}] - 2W_t^2 \exp{-(W_{20}/W_c)^2} \quad (3)$$

and

$$W_R^i = \frac{W_R}{\sin(i)} \quad . \quad (4)$$

W_t is the random motion component of the line width; $W_t = 38 \text{ km s}^{-1}$. W_c characterizes the transition region between linear and quadrature summation of rotational and dispersive terms; $W_c = 120 \text{ km s}^{-1}$. The formula degenerates to linear summation for giant galaxies, and quadrature summation for dwarf galaxies (Tully & Fouqué 1985). This correction for random motions decreases the line width of the local LCBG sample by 26 to 38 km s^{−1}, depending on the rotational velocity.

It is crucial, when comparing dynamical masses from different studies, that the rotational velocities be calculated in the same way. In general, we calculate the rotational velocities from W_R^i . However, when we wish to compare our sample with others (e.g. Roberts & Haynes 1994) who have not applied this correction for random motions to their line widths, we also do not apply this correction. We indicate dynamical masses calculated without correcting W_{20}^i for random motions as M_{DYN}^{NR} . Unless indicated as such, all dynamical masses are calculated using the line width corrected for random motions, W_R^i . Note that in all cases, the line widths have been corrected for inclination.

It is also crucial, when comparing dynamical masses from different studies, that they be measured within the same radius. Typically, the H I radius (R_{HI}) is measured at $1 \text{ M}_\odot \text{ pc}^{-2}$ and is used to estimate the total enclosed mass of a galaxy. However, it is only possible to measure R_{HI} with interferometers in nearby galaxies. By practical necessity then, some other radius must be adopted for our sample and the galaxy's mass is assumed to be spherically distributed in that radius. Two different radii are commonly used: R_e , the effective or

half-light radius, and R_{25} , the isophotal radius at the limiting surface brightness of 25 B-magnitudes arc sec^{-2} .

We have measurements of both R_e (in r and B band from SDSS) and R_{25} (in B-band from HyperLeda) for most galaxies. Vitores et al. (1996a,b) found that $R_{25} = 2.5 R_e$ for nearby emission line galaxies measured in r-band. When we compare our values of R_e to R_{25} , we find medians of

$$\left\langle \frac{R_{25}}{R_e(r)} \right\rangle = 4.1 \pm 0.7 \quad (5)$$

and

$$\left\langle \frac{R_{25}}{R_e(B)} \right\rangle = 4.0 \pm 0.9 . \quad (6)$$

For the galaxies with no R_{25} (SDSSJ0218–0757, SDSSJ0222–0830 and SDSSJ1118+6316) or R_e (non-SDSS galaxies) measurements available, we estimate these quantities from the above relations.

We find our local sample of LCBGs have dynamical masses, measured within R_{25} , ranging from 3×10^9 to $1 \times 10^{11} M_\odot$, with a median of $3 \times 10^{10} M_\odot$. The dynamical masses measured within the effective radius (measured in both the r and B-band) range from 8×10^8 to $3 \times 10^{10} M_\odot$, with a median of $8 \times 10^9 M_\odot$.

Figure 5 compares the dynamical masses measured for local LCBGs to nearby galaxies of Hubble type S0a through Im, where “m” indicates Magellanic, or low luminosity (Roberts & Haynes 1994). Note that Roberts & Haynes (1994) did not correct line widths for random motions as we did. Therefore, in Figure 5 we compare $M_{DYN}^{NR}(R < R_{25})$ which have not been corrected for random motions. These dynamical masses are higher than those we list in Table 3, which have been corrected for random motions. As seen in Figure 5, some local LCBGs have dynamical masses as large as L^* galaxies ($\sim 10^{11} M_\odot$, Roberts & Haynes 1994). However, at least 75% have dynamical masses approximately an order of magnitude smaller than typical local L^* galaxies, consistent with observations of LCBGs at higher redshifts (as discussed in § 1.1). However, our sample includes galaxies down to 0.25 L^* . Galaxies of this luminosity typically have dynamical masses (within R_{25}) $\sim 2 \times 10^{10} M_\odot$ (Roberts & Haynes 1994). Therefore, it is more appropriate to compare mass-to-light ratios; See §4.1.

We estimate the random errors associated with the dynamical masses to be approximately 50%. This estimate is made from uncertainties in the inclination ($\pm 12^\circ$, from the earlier comparison of HyperLeda and SDSS inclinations); uncertainties in radii measurements (as given by HyperLeda and SDSS); and uncertainties in measuring W_{20} (as discussed above). However, the random errors are overwhelmed by the systematic uncertainties when estimating dynamical masses. We have chosen a structural constant of $c_2 = 1$, but this could

be as high as 1.5, as discussed earlier. Even more significant is that 45% of our galaxy sample have other galaxies at similar velocities in the beam of the GBT. As the H I emission from all sources in the beam and within the bandwidth is blended into one spectrum, we may be overestimating the masses of these galaxies. Finally, a fifth of our galaxies have low inclinations ($< 40^\circ$) which lead to large corrections and therefore increasing uncertainties in the rotational velocities and overestimations of the dynamical masses. The dynamical masses we report may be viewed as upper limits – we are certainly overestimating the masses in many cases, but not underestimating them.

We are pursuing a follow-up program with both the Arecibo Radio Telescope and the VLA to address these issues. At 21 cm the Arecibo Radio Telescope has a beam size of $3'.1 \times 3'.5$, a third the size of the GBT beam. This decreases the number of target galaxies observed with other galaxies in the beam, decreasing the number of galaxies with overestimates of dynamical masses. We have already observed over 40 LCBGs at Arecibo, but results are not yet available. The VLA in “B” configuration provides the ability to map our galaxies in 21 cm emission to a resolution of $5''$. We have begun a survey of those LCBGs with companions. VLA maps allow us to disentangle the emission from each galaxy and more accurately estimate the dynamical mass of the target galaxy.

3.2. H I Content

Along with dynamical mass, a knowledge of the amount of fuel, i.e. atomic and molecular gas, available for the starburst activity, is critical for narrowing down the evolutionary possibilities for LCBGs. When combined with star formation rates, this gives an estimate of the maximum length of the starburst at the current rate of star formation. We defer a full discussion of this until Paper II (Garland et al. 2004) where we present our measurements of the CO content of these galaxies, but present the H I results here.

The H I masses are given by:

$$\frac{M_{HI}}{M_\odot} = 2.356 \times 10^5 \frac{D_{HI}^2}{Mpc^2} \int \frac{S \, dv}{Jy \, km \, s^{-1}} \quad (7)$$

(Roberts & Haynes 1994), where the distance (measured from H I) is $D = V_{BARY} H_o^{-1}$. The total H I flux, $\int S \, dv$, was calculated by numerically integrating under the spectrum where it is distinguishable from the noise. For the two marginal detections, SDSSJ0218–0757 and SDSSJ0222–0830, H I masses were calculated using the optical (SDSS) recessional velocities.

We find local LCBGs have H I masses ranging from 5×10^8 to $8 \times 10^9 M_\odot$, with a median of $5 \times 10^9 M_\odot$. These span the range of H I masses in nearby galaxies across the Hubble sequence;

the median is that of nearby late-type spiral galaxies (Roberts & Haynes 1994). The uncertainties listed for M_{HI} (Table 3) include uncertainties in the distance and integrated flux density, as listed in Table 2. However, as in the discussion of dynamical mass uncertainties in §3.1, the H I masses for nearly half of our galaxies are most likely overestimates due to the presence of other galaxies within the GBT beam.

4. Analysis

4.1. Mass-to-Light Ratios

Dynamical mass-to-light ratios indicate whether our local sample of LCBGs are undermassive for their luminosities. We calculated the total blue luminosities, L_B , of our galaxies from M_B , assuming $M_{B\odot} = 5.48$ (Roberts & Haynes 1994). We find the median mass-to-light ratio, $M_{DYN}(R < R_{25}) L_B^{-1} = 3 M_\odot L_{B\odot}^{-1}$, with a minimum of 0.6 and a maximum of $9 M_\odot L_{B\odot}^{-1}$.

Roberts & Haynes (1994) find that $M_{DYN}(R < R_{25}) L_B^{-1}$ ranges from $3.6 - 10 M_\odot L_{B\odot}^{-1}$ in local galaxies across the Hubble sequence. The median $M_{DYN}(R < R_{25}) L_B^{-1}$ is fairly constant ranging from 5 to $7 M_\odot L_{B\odot}^{-1}$. However, as discussed in §3.1, to compare our mass-to-light ratios to those of local, normal Hubble-types in Roberts & Haynes (1994), we must use dynamical masses which have not been corrected for random motions. Figure 6 compares such mass-to-light ratios for our local sample of LCBGs and nearby Hubble types. While some local LCBGs have mass-to-light ratios equal to or greater than the median for local Hubble types, approximately half the local LCBGs have smaller mass-to-light ratios. Many of the galaxies with mass-to-light ratios typical of local Hubble types have other galaxies within the beam, possibly leading to an overestimation of the dynamical mass-to-light ratio of the target galaxy. Therefore, in general, LCBGs tend to have mass-to-light ratios smaller than local normal galaxies. That is, most are small galaxies undergoing large amounts of star formation and not simply large galaxies with moderate amounts of star formation.

4.2. How gas-rich are LCBGs?

We calculated the gas mass fraction, $M_{HI} M_{DYN}^{-1} (R < R_{HI})$ for the local sample of LCBGs as a measure of their atomic gas richness. We do not have interferometric observations of these galaxies, so we estimated the hydrogen radius, R_{HI} , from optical radii. Broeils & van Woerden (1994) found for nearby spiral galaxies that $R_{HI} = 2 R_{25}$, where R_{HI} is measured at the $1 M_\odot \text{ pc}^{-2}$ level. However, van Zee, Skillman & Salzer (1998) found R_{HI}

ranging from $3 - 5 R_{25}$ for a small sample of local H II galaxies which are similar to LCBGs, but much less luminous ($M_B \gtrsim -16$). Martín (1998) studied a large sample of nearby galaxies and found that galaxies with smaller optical radii have larger H I extensions. Taylor et al. (1994) have measured R_{HI} in one of our LCBGs, Mrk 314, using the VLA. They find $R_{HI} = 4 R_{25}$. Therefore, although we estimated R_{HI} as $2 \times R_{25}$ following Broeils & van Woerden (1994), we note it may be an underestimate, which would cause us to overestimate the gas mass fraction. We are undertaking interferometric observations of some of our local sample of LCBGs to directly measure R_{HI} . This will be addressed in a future paper.

In local LCBGs, we find the gas mass fraction, $M_{HI} M_{DYN}^{-1}$, ranges from 0.03 to 0.2, with a median of 0.08. That is, it ranges from normal Hubble type spirals (< 0.1 (Roberts & Haynes 1994)) to very gas rich galaxies such as nearby H II and irregular galaxies studied by van Zee, Skillman & Salzer (1998) with gas fractions ranging from 0.2 – 0.4. This is similar to the range of 0.01 – 0.5 found by Pisano et al. (2001) for local blue compact galaxies, most of them less luminous than LCBGs.

The fraction of hydrogen mass to blue luminosity provides a distance independent alternative measure of the gas richness of galaxies. We find our local LCBGs have $M_{HI} L_B^{-1}$ ranging from 0.09 to $2 M_\odot L_{B\odot}^{-1}$, with a median of $0.4 M_\odot L_{B\odot}^{-1}$. This spans the range of nearby galaxies from S0a through Im, the median corresponding to late-type spirals (Roberts & Haynes 1994; Bettoni, Galletta & García-Burillo 2003). Gordon & Gottesman (1981) studied a range of blue compact galaxies, ranging from faint blue compact dwarfs to LCBGs, and found the same median value, $0.4 M_\odot L_{B\odot}^{-1}$.

4.3. The Tully-Fisher relationship and local LCBGs

The Tully-Fisher relationship, a relation between line width and luminosity, is a fundamental scaling relation for non-interacting spiral galaxies. An absolute blue magnitude versus H I line width version of the Tully-Fisher relationship is shown in Figure 7. We have compared our local LCBGs with the Tully-Fisher relation found for ~ 4500 normal galaxies within ~ 40 Mpc (Tully & Pierce 2000).

As seen in Figure 7, the location of local LCBGs is consistent with the Tully & Pierce (2000) relation, although with a large scatter. Tully & Pierce (2000) have a 1σ scatter of 0.3 magnitudes in M_B , while the local LCBGs have a 1σ scatter of 0.9 magnitudes in M_B . Approximately half the galaxies (without other sources in the beam) lie to the left of the Tully-Fisher relationship, indicating they have lower masses than expected from their luminosities, although this result is not statistically significant. This is consistent with the

distribution of LCBG and Hubble type galaxy mass-to-light ratios in Figure 6. Seven of the galaxies lying to the right of the Tully-Fisher relationship have other galaxies within the GBT beam, possibly leading to overestimations of the line widths.

Note that in our comparison of magnitudes, masses, and mass-to-light ratios, as in all other comparisons in this paper, we have adjusted all values to a Hubble constant of $H_0 = 70 \text{ km s}^{-1} \text{ Mpc}^{-1}$

5. Discussion: Comparison with Local Galaxy Types

We have observed 20 local LCBGs chosen with the same selection criteria as those LCBGs common at higher redshifts. LCBGs cannot remain LCBGs for a long period of time: The number density of LCBGs decreases by at least a factor of ten from $z > 0.5$ to today. That is, while LCBGs were common in the past, there are very few today. Out of approximately a million nearby galaxies observed by the SDSS, only about a hundred are LCBGs. (See Castander et al. 2004 for a discussion of the local space density of LCBGs.) Therefore, LCBGs must evolve into some other galaxy type.

From studies of intermediate redshift LCBGs, Koo et al. (1994) and Guzmán et al. (1996) proposed that some may be progenitors of local dwarf elliptical galaxies. Alternatively, Phillips et al. (1997) and Hammer et al. (2001) proposed that some may be disk galaxies in the process of forming a bulge to become present-day L* spiral galaxies. Two pieces of information are crucial to determining if these possibilities are likely. It is necessary to know the dynamical masses and the duration of the starbursts. We have measured the dynamical masses of our local sample of LCBGs using H I. The length of the starburst will not be estimated until we discuss our molecular gas survey in Paper II (Garland et al. 2004). However, we can use our measurements of line width and radius to identify local galaxies comparable to LCBGs, independent of the evolutionary stage of their stellar populations.

In Figure 8 we plot the effective or half-light radius, R_e , versus the velocity dispersion, σ , for our sample of local LCBGs, intermediate redshift ($0.4 \lesssim z \lesssim 1$) LCBGs (Guzmán et al. 1997; Phillips et al. 1997), and local samples of elliptical, spiral, Magellanic spiral, irregular, and dwarf elliptical galaxies (Guzmán et al. 1996; HyperLeda). We measured the σ of our sample of galaxies from the H I spectra by measuring the moments of the spectra. The measurements were made in the same way as we described in §3.2 for measuring $\int S dv$, the zeroth moment. We find similar results if we simply scale W_{20} to σ by assuming the spectra are Gaussian, that is, dividing W_{20} by 3.6. The values of σ for the other galaxy samples are from optical line width measurements, except the measurements for Magellanic spirals are

from 21 cm H I line widths. Optical line widths may be smaller than H I line widths. For example, Pisano et al. (2001) studied a sample of nearby blue compact galaxies and found the ionized gas emission line widths to be systematically smaller than the neutral hydrogen emission line widths. On average, the ratio of W_{20} measured from H II to W_{20} measured from H I was 0.66 for their sample of 11 blue compact galaxies. However, the galaxies in Pisano et al. (2001)’s sample tend to be smaller both in effective radius and H I line width than our sample of local LCBGs, suggesting that the difference between the optical and H I line widths may be smaller as well (Pisano et al. 2001; Martín 1998).

The R_e versus σ plot allows us to compare the dynamical mass properties of our sample of LCBGs with the other galaxy types. These properties are expected to remain constant despite luminosity evolution. We find that while some local LCBGs have σ consistent with local spiral galaxies, they tend to be too small in R_e . However, local LCBGs are consistent with the smaller spiral galaxies, Magellanic spirals. They are inconsistent with elliptical galaxies, but are consistent with the most massive dwarf elliptical and irregular galaxies. There is much confusion by what various authors mean when discussing dwarf elliptical galaxies (sometimes called spheroidal galaxies). We are referring to galaxies such as NGC 205 and *not* the less massive and less luminous galaxies like Draco and Carina. Finally, when we compare our local sample of LCBGs with those LCBGs observed at intermediate redshifts, we find that they occupy the same region of $R_e - \sigma$ space, suggesting we are indeed examining a similar mass range in both samples of galaxies.

We also compared local LCBGs to other galaxy types in $W_{20} \sin^{-1}(i)$ versus R_{25} space, where W_{20} was measured from H I emission for all samples. This allowed us to investigate if the wavelength used to measure the line width, or correcting the line width for inclination, was having an effect on our interpretation of which galaxy types most resemble LCBGs. We could only compare local LCBGs, spirals, Magellanic spirals, and irregular galaxies, as H I observations of intermediate redshift LCBGs and dwarf ellipticals are rare or non-existent. Our findings were entirely consistent with the interpretation from Figure 8.

Local LCBGs are therefore consistent with the dynamical mass properties of the most massive dwarf ellipticals and irregulars, and lower mass or Magellanic spirals. These classes vary in color and magnitude. Knowledge of the amount of molecular gas, time scale of starburst and fading, along with the ability of the galaxy to retain its interstellar medium, will allow us to discriminate between these remaining possibilities. We will begin this work in Paper II (Garland et al. 2004). Given the diverse nature of LCBGs, it is likely that multiple scenarios apply, each to a different subset of LCBGs.

6. Conclusions

We have performed a single dish 21 cm H I survey of 20 local LCBGs chosen to be local analogs to the numerous LCBGs studied at intermediate redshifts ($0.4 \lesssim z \lesssim 0.7$). Our findings have verified results from intermediate redshift LCBG studies. We have found that local LCBGs are a morphologically heterogeneous mixture of galaxies. They are typically gas-rich, with median values of $M_{HI} = 5 \times 10^9 M_{\odot}$ and $M_{HI} L_B^{-1} = 0.4 M_{\odot} L_{\odot}^{-1}$. Approximately half have mass-to-light ratios approximately ten times smaller than local galaxies of all Hubble types at similar luminosities, confirming that these are indeed small galaxies undergoing vigorous bursts of star formation. This proportion is likely an underestimate, as nearly half our sample of galaxies may have dynamical mass overestimates.

By comparing line widths and radii with local galaxy populations, we find that local LCBGs are consistent with Magellanic spirals, and the more massive irregulars and dwarf ellipticals. Measurements of the length of starburst, amount of fading, and ability of these galaxies to retain their interstellar media will help to constrain the evolutionary possibilities of this galaxy class. We begin to address these issues in Paper II (Garland et al. 2004), where we present the results of a molecular gas survey of these same local LCBGs.

Acknowledgments We thank the referee for helpful comments which improved the quality of this paper. We thank Rick Fisher for providing the H I spectrum of SDSSJ0934+0014. We also thank the operators and staff at the GBT for their help with the observing and reduction, and their hospitality. Support for this work was provided by the NSF through award GSSP02-0001 from the NRAO. D. J. P. acknowledges generous support from an NSF MPS Distinguished International Postdoctoral Research Fellowship, NSF Grant AST0104439. R. G. acknowledges funding from NASA grant LTSA NAG5-11635. Funding for the creation and distribution of the SDSS Archive has been provided by the Alfred P. Sloan Foundation, the Participating Institutions, the National Aeronautics and Space Administration, the National Science Foundation, the U.S. Department of Energy, the Japanese Monbukagakusho, and the Max Planck Society. The SDSS Web site is <http://www.sdss.org/>. We have made extensive use of HyperLeda (<http://www-obs.univ-lyon1.fr/hypercat/>) and the NASA/IPAC Extragalactic Database (NED) which is operated by the Jet Propulsion Laboratory, California Institute of Technology, under contract with the National Aeronautics and Space Administration (<http://nedwww.ipac.caltech.edu/>). The Digitized Sky Surveys were produced at the Space Telescope Science Institute under U.S. Government grant NAG W-2166. The images of these surveys are based on photographic data obtained using the Oschin Schmidt Telescope on Palomar Mountain and the UK Schmidt Telescope.

REFERENCES

Barton, E. J. & van Zee, L. 2001, ApJ, 550, L35

Bender, R., Burstein, D., & Faber, S. M. 1992, ApJ, 399, 462

Bettoni, D., Galletta, G., & García-Burillo, S. 2003, A&A, 405, 5

Bergvall, N. & Östlin, G. 2002, A&A, 390, 891

Broeils, A. H. & van Woerden, H. 1994, A&AS, 107, 129

Calzetti, D. 1997, AJ, 113, 162

Campos-Aguilar, A., Moles, M., Masegosa, J. 1993 AJ 106 1784

Castander, F. J. et al. 2004, in preparation

de Vaucouleurs G., Vaucouleurs A. de, Corwin H.G. Jr., Buta R.J., Paturel G., & Fouqué P. Third Reference Catalogue of Bright Galaxies, 1991 (New York: Springer-Verlag)

Doublier, V., Comte, G., Petrosian, A., Surace, C., & Turatto, M. 1997, A&AS, 124, 405

Fisher, R. 2003, http://www.gb.nrao.edu/~rfisher/GalaxySurvey/galaxy_survey.html

Garland, C. A. et al. 2004, in preparation

Giavalisco, M., Steidel, C. C., & Macchetto, F. D. 1996, ApJ, 470, 189

Gordon, D. & Gottesman, S. T. 1981, AJ, 86, 161

Guzmán, R., Gallego, J., Koo, D. C., Phillips, A. C., Lowenthal, J. D., Faber, S. M., Illingworth, G. D., & Vogt, N. P. 1997, ApJ, 489, 559

Guzmán, R., Koo, D. C., Faber, S. M., Illingworth, G. D., Takamiya, M., Kron, R., & Bershady, M. A. 1996, ApJ, 460, L5

Guzmán, R., Koo, D. C., Jangren, A., Bershady, M., Faber, S. M., & Illingworth, G. D. 1998, ApJ, 495, L13

Hammer, F., Gruel, N., Thuan, T. X., Flores, H., & Infante, L. 2001, ApJ, 550, 570

Hunter, D. A. & Gallagher, J. S. 1986, PASP, 98, 5

Jangren, A., Bershady, M. A., Conselice, C., Koo, D. C., & Guzmán, R. 2004, AJ, submitted

Kong, X. & Cheng, F. Z. 2002, A&A, 389, 845

Koo, D. C., Bershady, M. A., Wirth, G. D., Stanford, S. A., & Majewski, S. R. 1994, ApJ, 427, L9

Lilly, S., Schade, D., Ellis, R., Le Fevre, O., Brinchmann, J., Tresse, L., Abraham, R., Hammer, F., Crampton, D., Colless, M., Glazebrook, K., Mallén-Ornelas, G., & Broadhurst, T. 1998, ApJ, 500, 75

Lockman, L. J. 1998, Proc. SPIE, 3357, 656

Lowenthal, J. D., Koo, D. C., Guzmán, R., Gallego, J., Phillips, A. C., Faber, S. M., Vogt, N. P., Illingworth, G. D., & Gronwall, C. 1997, ApJ, 481, 673

Mallén-Ornelas, G., Lilly, S. J., Crampton, D., & Schade, D. 1999, ApJ, 518, 83

Martín, M. C. 1998, A&AS, 131, 77

Marzke, R. O., Geller, J. J., Huchra, J. P., Harold, G., & Corwin, J. 1994, AJ, 108, 437

Ott, M., Witzel, A., Quirrenbach, A., Krichbaum, T. P., Standke, K. J., Schalinski, C. J., & Hummel, C. A. 1994, A&A, 284, 331

Phillips, A. C., Guzmán, R., Gallego, J., Koo, D. C., Lowenthal, J. D., Vogt, N. P., Faber, S. M., & Illingworth, G. D. 1997, ApJ, 489, 543

Pisano, D. J., Kobulnicky, H. A., Guzmán, R., Gallego, J., & Bershady, M. A. 2001, AJ, 122, 1194

Poggianti, B. M. 1997, A&AS, 122, 399

Richter, O.-G. & Sancisi, R. 1994, A&A, 290, L9

Roberts, M. S. & Haynes, M. P. 1994, ARA&A, 32, 115

Sargent, W. L. W. 1970, ApJ, 160, 405

Smail, I., Ivison, R. J., Blain, A. W., & Kneib, J.-P. 1998, ApJ, 507, L21

Stoughton, C. et al. 2002, AJ, 123, 485

Taylor, C. L., Brinks, E., Pogge, R. W., & Skillman, E. D. 1994 AJ, 107, 971

Thuan, T. X. & Martin, G. E. 1981, ApJ, 247, 823

Tully, R. B. & Fouqué, P. 1985, *ApJS*, 58, 67

Tully, R. B. & Pierce, M. M. 2000, *ApJ*, 533, 744

van Zee, L., Skillman, E. D., & Salzer, J. J. 1998, *AJ*, 116, 1186

Vitores, A. G., Zamorano, J., Rego, M., Alonso, O. & Gallego, J. 1996a, *A&AS*, 118, 7

Vitores, A. G., Zamorano, J., Rego, M., Gallego, J., & Alonso, O. 1996b, *A&AS*, 120, 385

Weedman, D. W., Wolovitz, J. B., Bershady, M. A., & Schneider, D. P. 1998, *ApJ*, 116, 1643

York, D. et al. 2000, *AJ*, 120, 1579

Zwicky, F. 1964, *ApJ*, 140, 1467

Table 1. Local LCBG Properties

Source	Alternate Names	D_{OPT} (Mpc)	M_B	B–V	SBe (B-mag arc sec $^{-2}$)	NED Type	HyperLeda Type	Other Sources in Beam?
Mrk 297	NGC 6052, NGC 6064	67	–21.0	0.4	20.6		Sc	y
Mrk 314	NGC 7468	30	–18.5	0.4	20.2	E3, pec (polar ring?)	E	n
Mrk 325	NGC 7673, Mrk 325	49	–20.0	0.4	20.0	SAC?, pec, H II starburst	Sc	y
Mrk 538	NGC 7714	40	–20.1	0.4	20.2	SB(s)b, pec, H II liner	SBb	y
SDSS J011932.95+145219.0	NGC 469	59	–18.9	0.4	20.3			y
SDSS J021808.75–075718.0		69	–18.8	0.5	20.2			n
SDSS J022211.96–083036.2		67	–18.6	0.4	20.1			n
SDSS J072849.75+353255.2		56	–18.9	0.4	20.3	S?	Sbc	n
SDSS J083431.70+013957.9		59	–19.1	0.6	20.6	SB(s)b	SBb	y
SDSS J090433.53+513651.1	Mrk 101	68	–19.7	0.6	20.3	S	Sc	n
SDSS J091139.74+463823.0	Mrk 102	61	–19.3	0.5	19.1	S?		n
SDSS J093410.52+001430.2	Mrk 1233	70	–19.8	0.3	19.9	Sb	Sbc	y
SDSS J093635.36+010659.8		71	–19.1	0.6	21.0			y
SDSS J094302.60–021508.9		68	–19.3	0.5	20.4	S0	S0	n
SDSS J111836.35+631650.4	Mrk 165	46	–18.6	0.4	19.4	compact starburst		n
SDSS J123440.89+031925.1	NGC 4538	67	–19.2	0.6	21.0	S pec	Sbc	n
SDSS J131949.93+520341.1		67	–18.7	0.2	20.1			y
SDSS J140203.52+095545.6	NGC 5414, Mrk 800	61	–19.7	0.5	19.7	pec		y
SDSS J150748.33+551108.6		48	–18.9	0.4	20.8	S	Sbc	n
SDSS J231736.39+140004.3	NGC 7580, Mrk 318	63	–19.3	0.6	20.4	S?	Sbc	n

Table 2. Local LCBG H I Line Measurements

Source	V_{BARY} (km s $^{-1}$)	D (Mpc)	W_{20} (km s $^{-1}$)	$\int S dv$ (Jy km s $^{-1}$)
Mrk 297	4739 ± 17	68 ± 0.2	362 ± 17	6.5 ± 0.08
Mrk 314	2081 ± 17	30 ± 0.2	188 ± 17	12 ± 0.1
Mrk 325	3427 ± 17	49 ± 0.2	202 ± 17	11 ± 0.2
Mrk 538	2798 ± 17	40 ± 0.2	240 ± 17	20 ± 0.2
SDSSJ0119+1452	4098 ± 17	59 ± 0.2	266 ± 17	2.4 ± 0.1
SDSSJ0218–0757				0.41 ± 0.07
SDSSJ0222–0830				0.61 ± 0.09
SDSSJ0728+3532	3953 ± 17	56 ± 0.2	216 ± 17	7.9 ± 0.1
SDSSJ0834+0139	4215 ± 160	60 ± 2	329 ± 160	6.9 ± 0.2
SDSSJ0904+5136	4782 ± 103	68 ± 2	204 ± 103	4.5 ± 0.2
SDSSJ0911+4636	4281 ± 17	61 ± 0.2	151 ± 17	2.0 ± 0.1
SDSSJ0934+0014	4860 ± 17	69 ± 0.2	332 ± 17	4.8 ± 0.2
SDSSJ0936+0106	4920 ± 17	70 ± 0.2	255 ± 17	3.3 ± 0.09
SDSSJ0943–0215	4823 ± 17	69 ± 0.2	230 ± 17	2.6 ± 0.06
SDSSJ1118+6316	3218 ± 17	46 ± 0.2	152 ± 17	2.2 ± 0.07
SDSSJ1234+0319	4685 ± 17	67 ± 0.2	269 ± 17	4.4 ± 0.1
SDSSJ1319+5203	4619 ± 17	66 ± 0.2	202 ± 17	7.7 ± 0.09
SDSSJ1402+0955	4267 ± 17	61 ± 0.2	343 ± 17	6.8 ± 0.2
SDSSJ1507+5511	3373 ± 17	48 ± 0.2	126 ± 17	3.7 ± 0.1
SDSSJ2317+1400	4413 ± 17	63 ± 0.2	254 ± 17	6.2 ± 0.1

^aMarginal detection; no line width measurements.

Table 3. Derived Parameters for Local LCBGs

Source	M_{HI} ($10^9 M_{\odot}$)	Inclination ($^{\circ}$)	W_R^i (km s $^{-1}$)	V_{ROT} (km s $^{-1}$)	$R_{25}(B)$ (kpc)	M_{DYN} ($R < R_{25}(B)$) ($10^{10} M_{\odot}$)	$R_e(r)$ (kpc)	M_{DYN} ($R < R_e(r)$) ($10^{10} M_{\odot}$)
Mrk 297	7.0 ± 0.1	42^a	486	243	8.0	11	2.0^c	2.7
Mrk 314	2.5 ± 0.05	65^a	170	85	3.8	0.63	0.94^c	0.16
Mrk 325	6.3 ± 0.1	43^a	242	121	9.6	3.3	2.4^c	0.83
Mrk 538	7.6 ± 0.1	50^a	264	132	11	4.5	2.8^c	1.1
SDSSJ0119+1452	2.0 ± 0.1	84	230	115	5.6	1.7	1.6	0.48
SDSSJ0218-0757	0.47 ± 0.08	52			4.9^b		1.3	
SDSSJ0222-0830	0.65 ± 0.1	48			4.2^b		1.2	
SDSSJ0728+3532	6.0 ± 0.1	34	321	160	5.4	3.3	1.2	0.74
SDSSJ0834+0139	5.9 ± 0.5	83	293	147	6.5	3.3	1.6	0.82
SDSSJ0904+5136	4.9 ± 0.3	34	301	150	7.4	3.9	2.0	1.0
SDSSJ0911+4636	1.7 ± 0.1	33	221	111	5.6	1.6	1.2	0.35
SDSSJ0934+0014	5.4 ± 0.2	51	378	189	6.8	5.7	1.9	1.5
SDSSJ0936+0106	3.8 ± 0.1	48	293	146	7.1	3.5	2.0	1.0
SDSSJ0943-0215	2.9 ± 0.07	84	194	97	4.9	1.1	1.8	0.39
SDSSJ1118+6316	1.1 ± 0.04	82	123	61	3.1^b	0.27	0.91	0.08
SDSSJ1234+0319	4.7 ± 0.1	52	293	147	6.7	3.4	2.1	1.1
SDSSJ1319+5203	7.9 ± 0.1	44	239	120	5.3	1.8	1.2	0.41
SDSSJ1402+0955	6.0 ± 0.2	55	372	186	8.7	7.0	1.6	1.3
SDSSJ1507+5511	2.0 ± 0.07	44	144	72	7.9	0.95	1.8	0.21
SDSSJ2317+1400	5.8 ± 0.1	31	420	210	7.3	7.5	1.7	1.8

^afrom HyperLeda

^bestimated as $4 \times R_e(B)$
^cestimated as $0.25 \times R_{25}$

Table 4. Additional Derived Parameters for Local LCBGs

Source	$M_{HI} M_{DYN}^{-1} (R < R_{HI})$	L_B ($10^9 L_\odot$)	$M_{HI} L_B^{-1}$ ($M_\odot L_\odot^{-1}$)	$M_{DYN} (R < R_{25}) L_B^{-1}$ ($M_\odot L_\odot^{-1}$)	$M_{DYN} (R < R_e) L_B^{-1}$ ($M_\odot L_\odot^{-1}$)
Mrk 297	0.03	39	0.2	3	0.7
Mrk 314	0.2	3.9	0.7	2	0.4
Mrk 325	0.1	16	0.4	2	0.5
Mrk 538	0.08	17	0.5	3	0.7
SDSSJ0119+1452	0.06	5.6	0.4	3	0.9
SDSSJ0218-0757		5.2	0.09		
SDSSJ0222-0830		4.3	0.2		
SDSSJ0728+3532	0.09	5.6	1	6	1
SDSSJ0834+0139	0.1	6.8	0.9	5	1
SDSSJ0904+5136	0.07	12	0.4	3	0.9
SDSSJ0911+4636	0.05	8.2	0.2	2	0.4
SDSSJ0934+0014	0.05	13	0.4	4	1
SDSSJ0936+0106	0.06	6.8	0.6	5	2
SDSSJ0943-0215	0.1	8.2	0.4	1	0.5
SDSSJ1118+6316	0.2	4.3	0.3	0.6	0.2
SDSSJ1234+0319	0.07	7.4	0.6	5	1
SDSSJ1319+5203	0.2	4.7	2	4	0.9
SDSSJ1402+0955	0.04	12	0.5	6	1
SDSSJ1507+5511	0.1	5.6	0.4	2	0.4
SDSSJ2317+1400	0.04	8.2	0.7	9	2

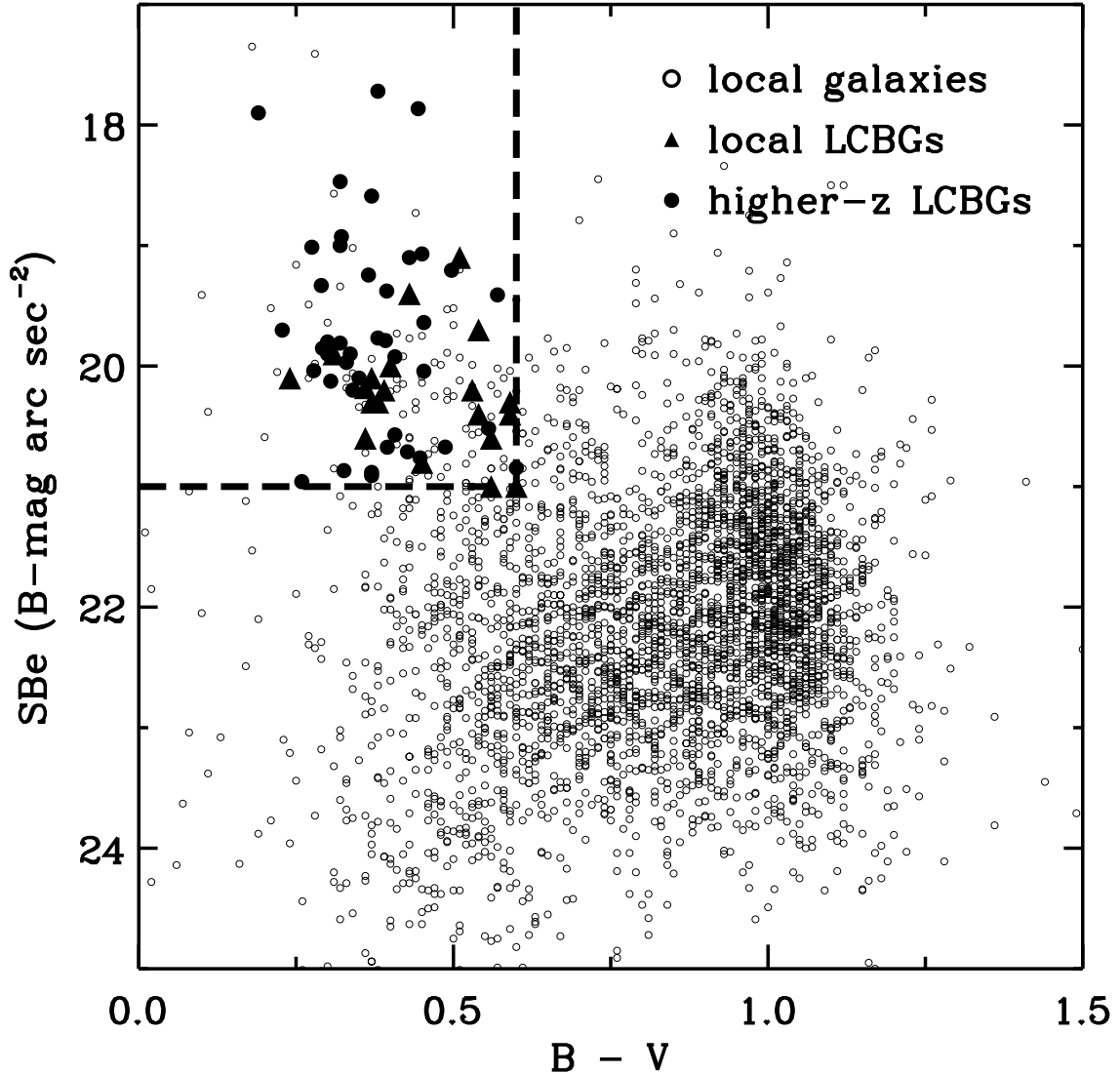


Fig. 1.— $B - V$ color versus SBe , average surface brightness within the effective radius (B -mag arc sec $^{-2}$), for three samples of galaxies. Open circles show the properties of ~ 4000 galaxies in the local Universe (HyperLeda); filled circles represent our local sample of galaxies which were selected with the same criteria used to define intermediate redshift LCBGs; triangles show a small sample of LCBGs at higher redshifts ($0.4 \lesssim z \lesssim 1$) observed by Koo et al. (1994), Guzmán et al. (1997, 1998), and Phillips et al. (1997). The dotted lines roughly demarcate the color and surface brightness criteria from Jangren et al. (2004) which separate LCBGs from normal galaxies. Compared to other galaxy types which dominate today's galaxy population, LCBGs are relatively rare in the nearby Universe.

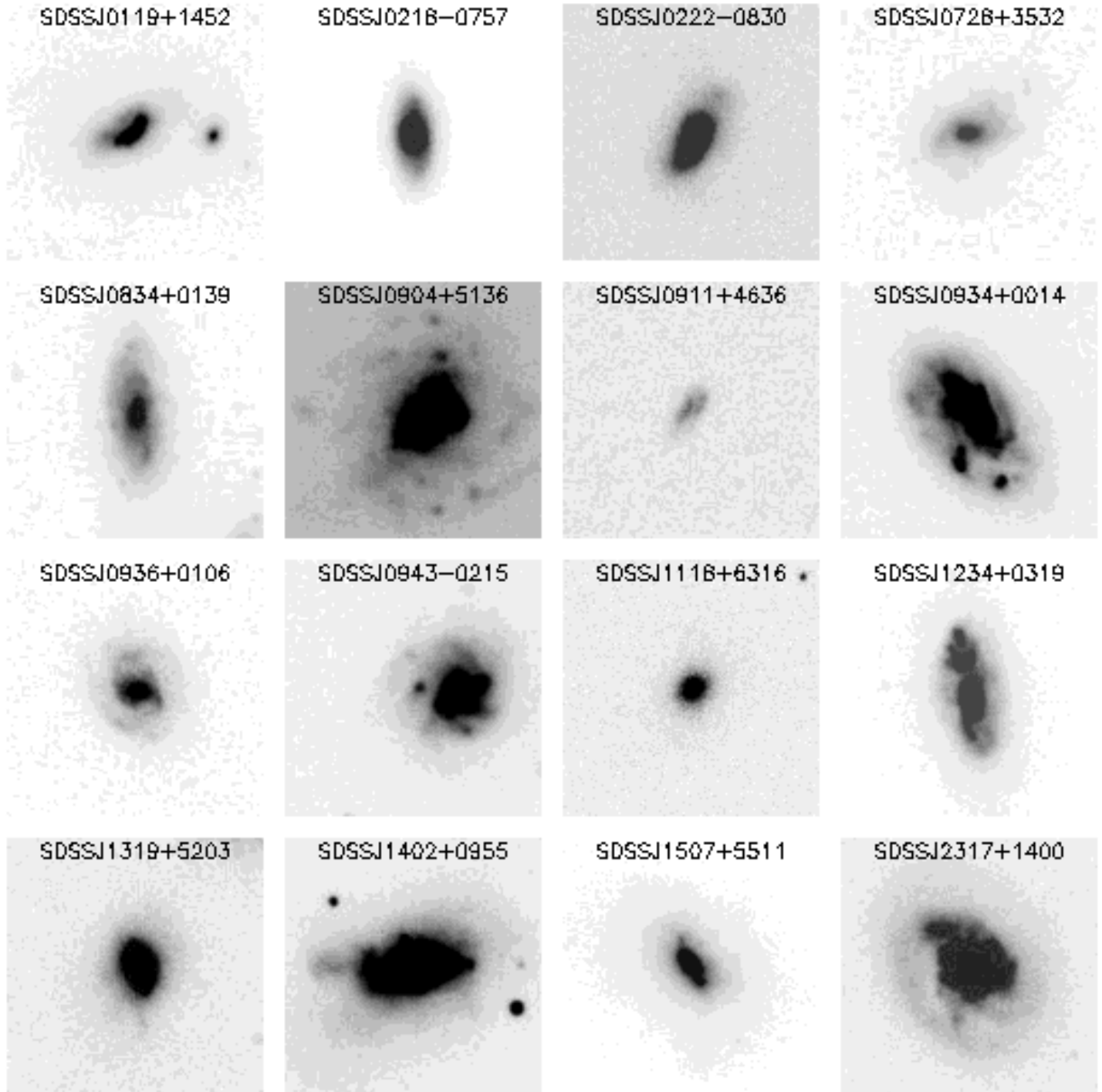


Fig. 2.— SDSS g-band (4770 Å) images of the 16 SDSS local LCBGs. Each image is 15 kpc in diameter. LCBGs are clearly morphologically heterogeneous.

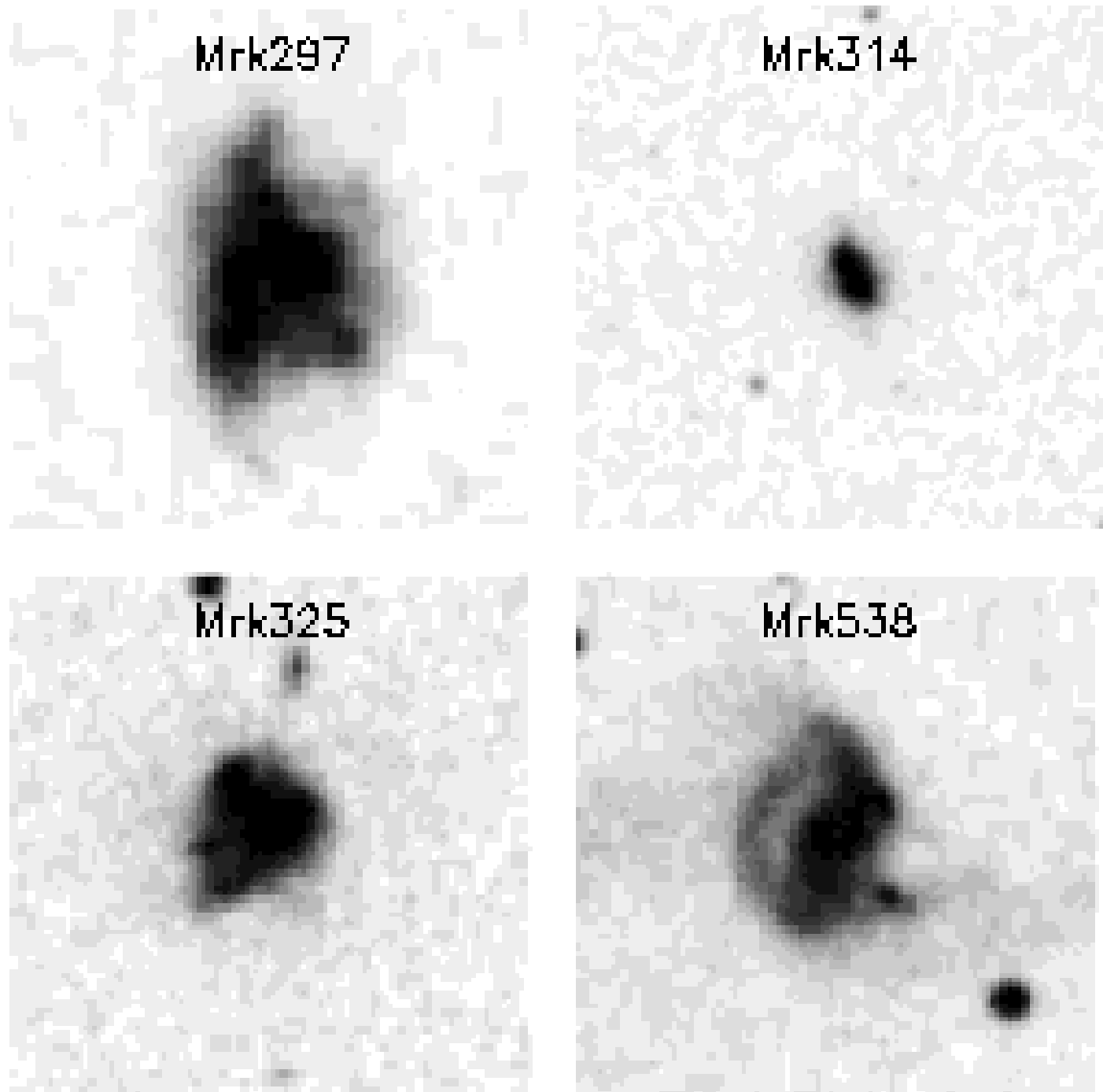


Fig. 3.— Digitized Sky Survey images of the four non-SDSS local LCBGs. Each image is 35 kpc in diameter.

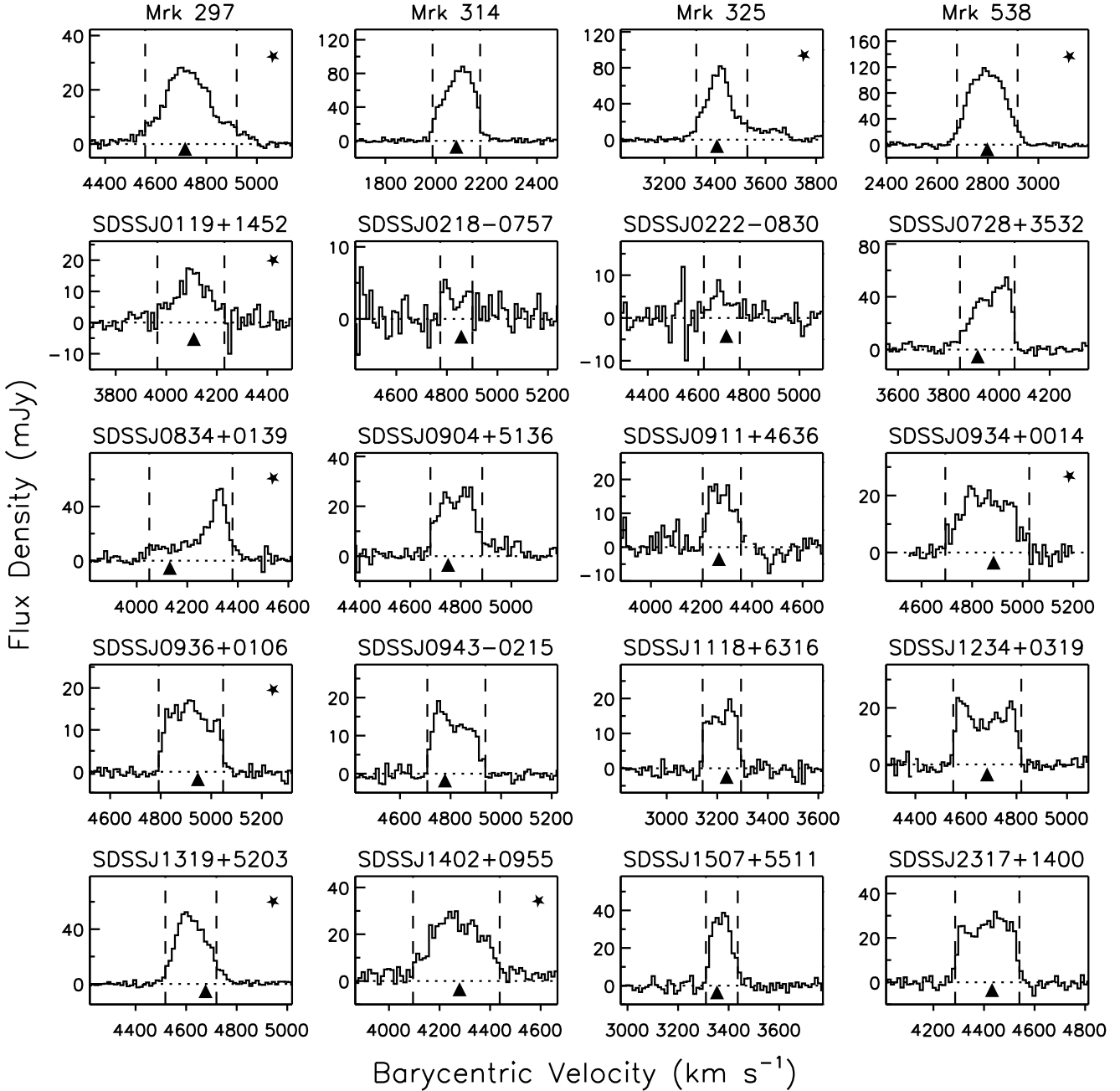


Fig. 4.— GBT H I spectra of the sample of nearby LCBGs. The vertical scales are flux densities, in mJy; the horizontal scales are barycentric velocities, in km s⁻¹. The spectra have been smoothed to a resolution of ~ 12 km s⁻¹ and only the central 800 km s⁻¹ are shown. The dashed lines indicate the 20% crossings used to measure the line width at 20%. The triangles indicate the recession velocities calculated from SDSS redshifts for the SDSS galaxies; velocities from NED redshifts are shown for the non-SDSS galaxies. Those galaxies with other sources at similar velocities within the GBT beam are indicated by a star in the upper right corner.

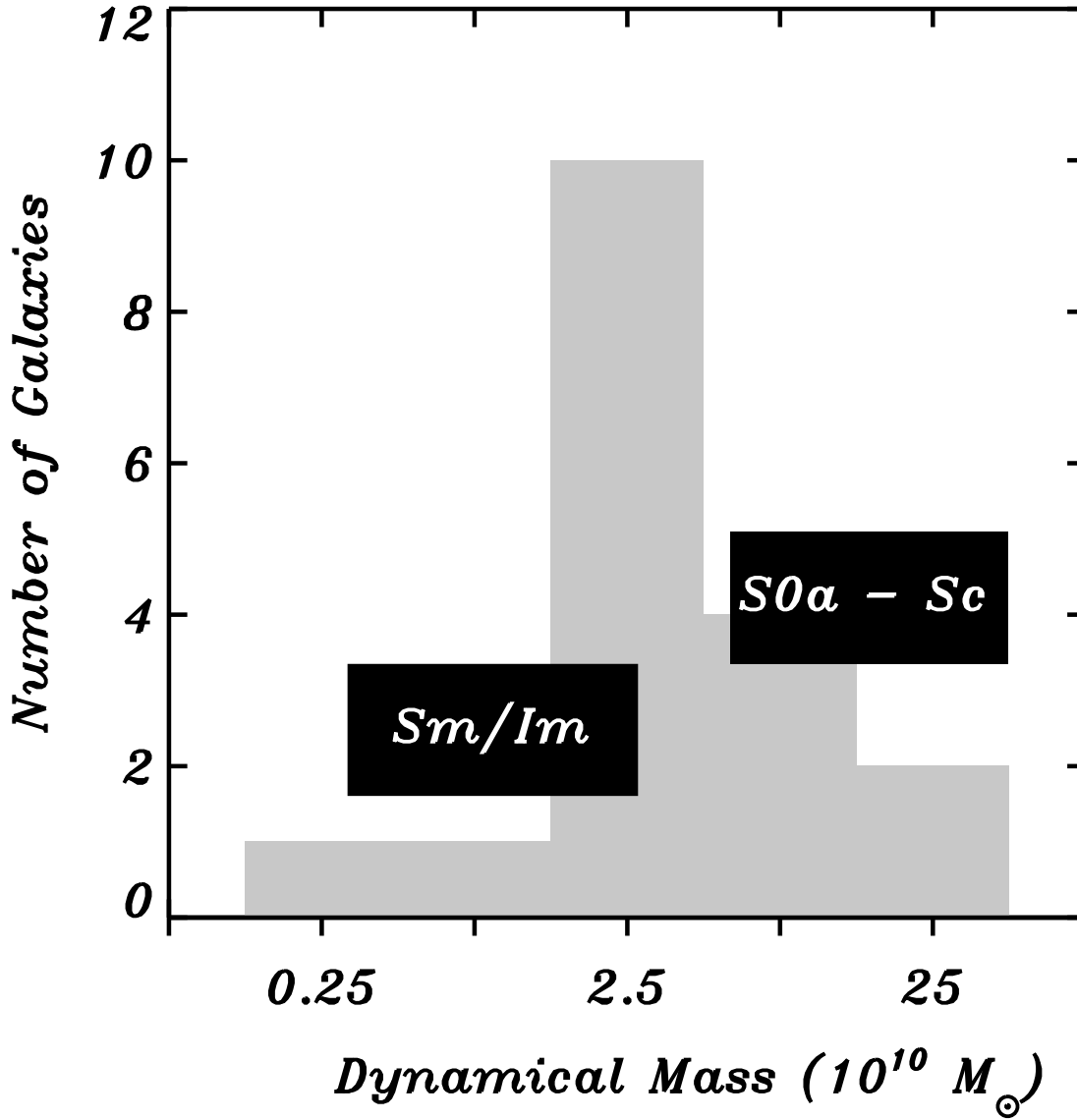


Fig. 5.— The distribution of dynamical masses, $M_{DYN}^{NR}(R < R_{25})$, for local LCBGs, as measured from H I observations, is shown as a gray histogram. For comparison, the range of dynamical masses for local Hubble type galaxies are indicated with black boxes. The “m” in “Sm” and “Im” indicates Magellanic or low-luminosity spirals and irregulars. Note that in order to compare LCBG dynamical masses with Roberts & Haynes (1994)’s results for local Hubble types, the dynamical masses plotted here do not include a line width correction for random motions.

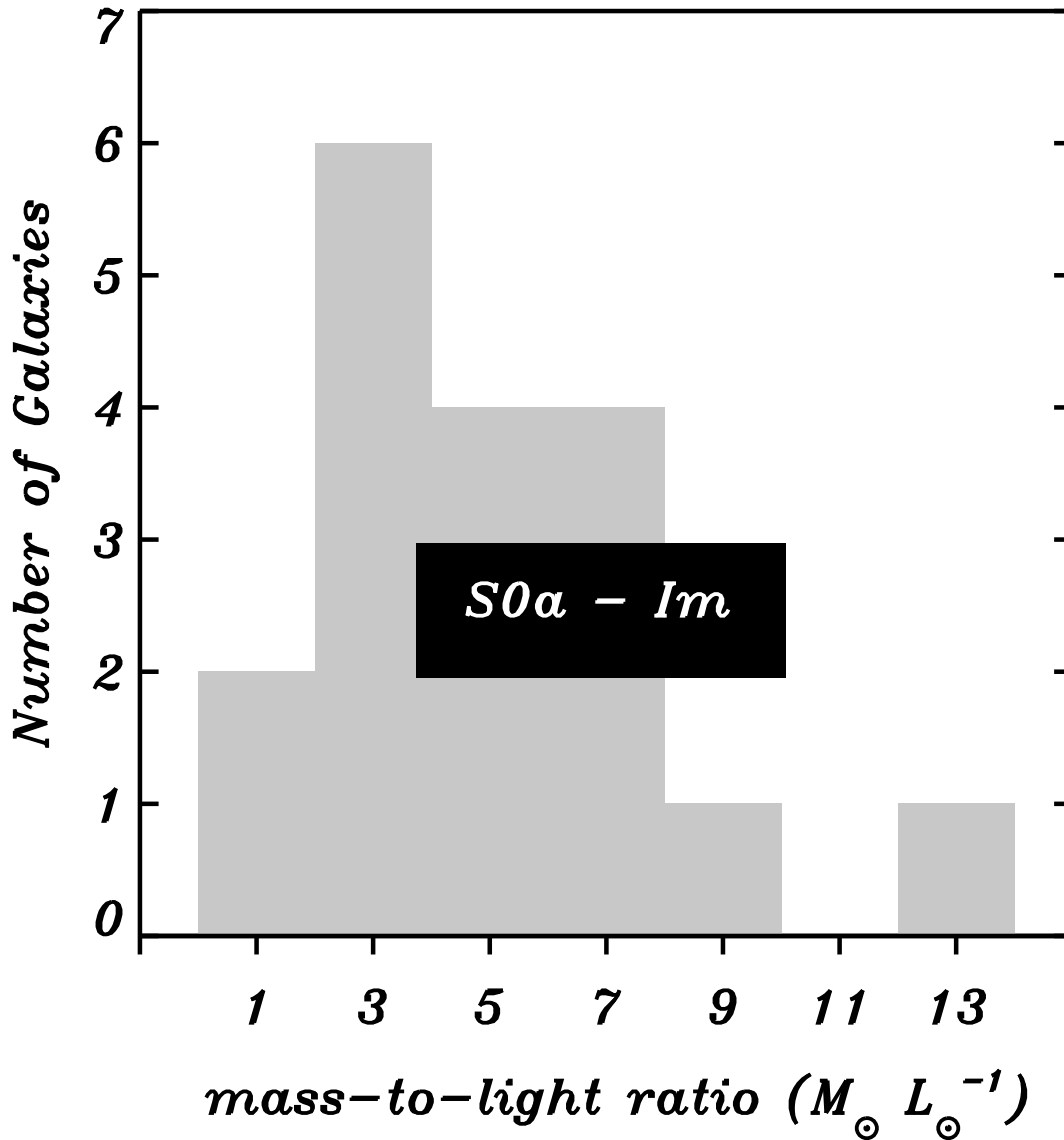


Fig. 6.— The distribution of dynamical mass (within R_{25}) to L_B ratios for local LCBGs is shown as a gray histogram. For comparison, the range of mass-to-light ratios for local Hubble type galaxies (S0a to Im) (Roberts & Haynes 1994) are shown. As in Figure 5, for accurate comparisons, these mass-to-light ratios do not include a line width correction for random motions. Many LCBGs tend to have mass-to-light ratios smaller than local normal galaxies, consistent with findings at intermediate redshifts. Note that we may have overestimated the dynamical masses for most of the LCBGs with higher mass-to-light ratios.

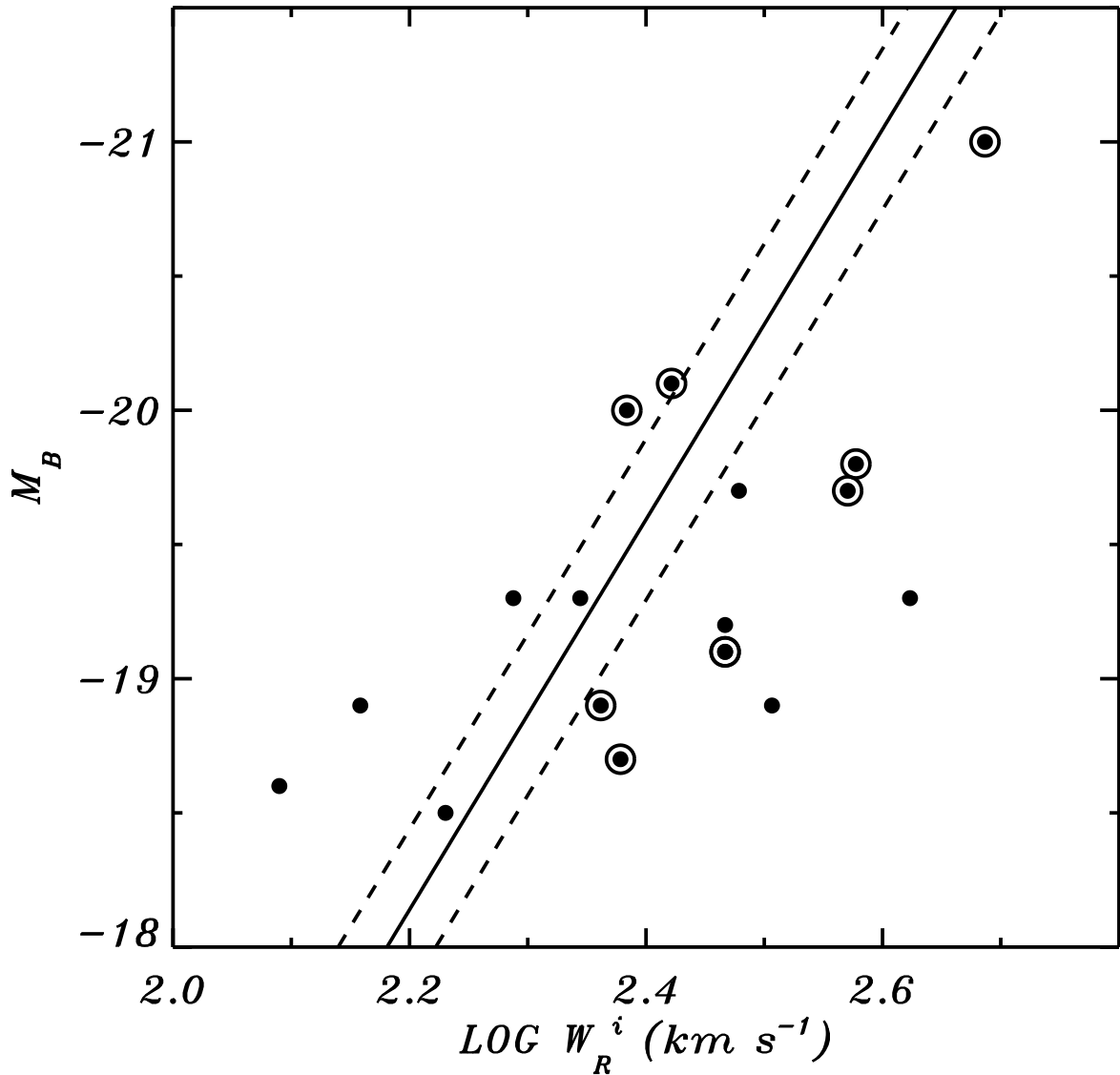


Fig. 7.— The Tully-Fisher distribution: the logarithm of the line width at 20% corrected for inclination and random motions (W_R^i) versus absolute blue magnitude (M_B). Local LCBGs are indicated by filled circles. Those galaxies with other sources at similar velocities within the GBT beam are circled; their line widths may be overestimated. The solid line indicates the Tully-Fisher relationship from Tully & Pierce (2000); the dotted lines indicate their 1σ scatter of $0.3 M_B$. The location of our local LCBGs is consistent with the Tully-Fisher relationship, but with a higher 1σ scatter of $0.9 M_B$.

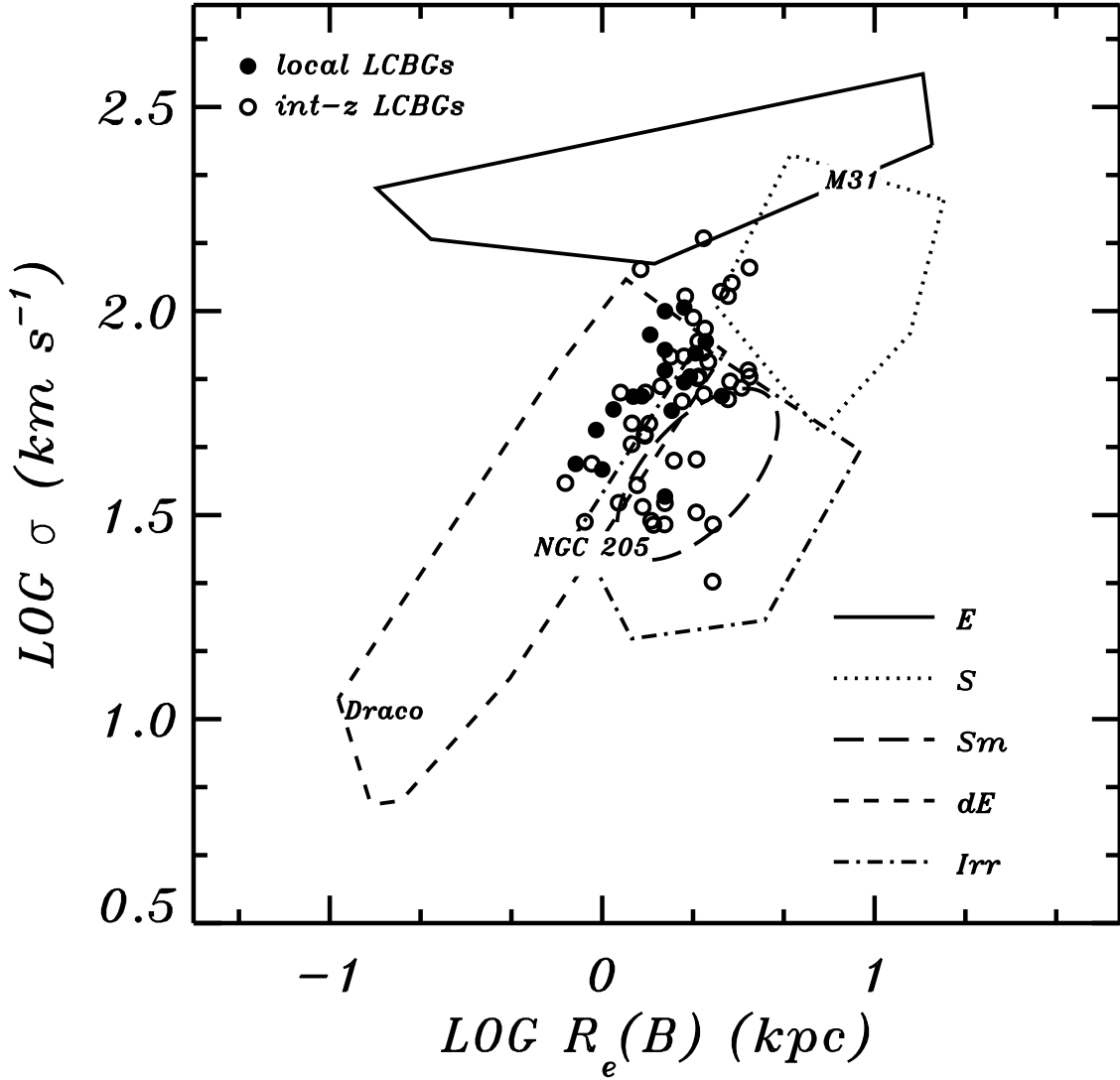


Fig. 8.— The effective radius (R_e) versus the the velocity dispersion (σ) is plotted for our local LCBGs (filled circles) and intermediate redshift ($0.4 \lesssim z \lesssim 1$) LCBGs (open circles) (Guzmán et al. 1997; Phillips et al. 1997). The regions occupied by the bulk of other local galaxy types—ellipticals (E), spirals (S), Magellanic spirals (Sm), dwarf ellipticals (dE), and irregulars (Irr)—are indicated (Guzmán et al. 1996, HyperLeda). We have also indicated the approximate locations for some representative galaxies: Draco, NGC 205 and M 31 (HyperLeda). Local LCBGs are consistent with higher mass irregulars and dwarf ellipticals, and lower mass or Magellanic spirals, as well as intermediate redshift LCBGs.